Scilight

Journal of Innovations in Materials and Manufacturing Engineering
https://www.sciltp.com/journals/jimme

Article

Evaluation of Solid-State Diffusion Bonded Inconel 718 Mechanical Properties

Leila Ladani [1] and Preston Regg Angell [1,2,*]

[1] Department of Materials Science and Engineering, Ira A. Fulton Schools of Engineering, Arizona State University, Tempe, AZ 85281, USA
[2] Honeywell Aerospace, Tempe, AZ 85284, USA
* Correspondence: prangell@asu.edu

How To Cite: Ladani, L.; Angell, P.R. Evaluation of Solid-State Diffusion Bonded Inconel 718 Mechanical Properties. *Journal of Innovations in Materials and Manufacturing Engineering* **2026**, *1*(1), 4.

Received: 9 October 2025
Revised: 15 February 2026
Accepted: 23 February 2026
Published: 10 March 2026

Abstract: Nickel based polycrystalline superalloys, designed for high temperature applications, are extensively used in the aerospace industry for the materials excellent mechanical properties at elevated temperatures. The relatively low intrinsic diffusivity of nickel-based alloys make them infamously difficult to diffusion bond. This study attempts to experimentally achieve solid state bonding of nickel-based superalloys, without the aid of an interlayer material, with complete grain coalescence while maintaining tensile properties of the base material. A design of experiments was conducted using Inconel 718 as base material bonded to itself in a hot press vacuum furnace, while key process parameters are iteratively varied. Mechanical properties of diffusion welded samples, subjected to a precipitation heat treatment, were compared against base material properties with the same precipitation heat treatment. The data collected indicates that diffusion bonding atmosphere, surface preparation, and thermal cycle are significant contributors in maintaining tensile properties. Tensile strength results of diffusion bonded samples were approximately 10–30% lower than the base material. The low tensile values are theorized to be a result of grain growth as outlined by the Hall-Petch theory. Elevated temperatures promote diffusion aiding successful bonding but also foster grain growth and coarsening of undesired secondary precipitates.

Keywords: solid state diffusion welding; nickel based precipitation hardenable alloys; mechanical properties

1. Introduction

Diffusion bonding is defined as the process of bonding materials in solid state to make a monolithic joint at the atomic level. This novelty process is achieved through intimate contact of mating surfaces at elevated temperatures and under pressure to cause plastic deformation [1]. Maitland et al. listed advantages of diffusion welding as: extremely high-quality joints, ability to achieve uniform mechanical properties similar to the optimized base material, the ability to join dissimilar metals, and little to no distortion. Some of the process's disadvantages noted were high tooling and development costs, long processing times, and complex quality assurance processes [2]. A comprehensive study conducted by Garrett, et al. outlines the essential variables of solid-state bonding as: substrate surface finish, process temperature, atmosphere control, applied pressure, and materials weldability. Their broad analysis covered typical processes applications and common challenges associated with the process [3]. This solid-state welding process leverages Fick's laws of diffusion to create a metallurgical bond making the two materials nearly indistinguishable at a microscopic level.

For interdiffusion of atoms to occur, the substrate surfaces must come in contact at atomic levels. Theoretically, two perfectly flat clean surfaces would spontaneously bond without any additional energy applied if brought into contact with one another [1]. In reality, extensive spontaneous bonding is largely unachievable due

Copyright: © 2026 by the authors. This is an open access article under the terms and conditions of the Creative Commons Attribution (CC BY) license (https://creativecommons.org/licenses/by/4.0/).
Publisher's Note: Scilight stays neutral with regard to jurisdictional claims in published maps and institutional affiliations.

to microscopic peaks and valleys present on even the best surface polishes. Macroscopic surface alignment, affecting surfaces contacting, is also another factor to be considered. Additionally, oxides and contaminants inhibit diffusion between substrates [2]. Extreme measures must be taken to minimize these barriers.

Some of the challenges associated with surface imperfections may be overcome by using high temperature and pressure. Hypothetically, using elevated temperatures and pressure causes plastic deformation of the surfaces closing the gaps caused by the surface imperfections. This close contact provides an opportunity for atoms to cross the interface via diffusion. High temperatures also increase the mobility of atoms and enhance interdiffusion. Porter et al. outlined the jump rate of substitutional diffusing atoms and mathematically modeled the phenomena with the modified Arrhenius equation (shown in Equation (1)) [4,5].

$$\Gamma = vzX_v e^{\left(-\frac{\Delta G}{k_B T}\right)} \tag{1}$$

where

$$\Gamma = \text{Jump rate}$$

$$\Delta G = \text{Change in Gibbs Free Energy}$$

$$T = \text{Absolute temperature}$$

$$K_B = \text{Boltzmanns constant}$$

$$v = \text{Average vibation frequency}$$

$$z = \text{Nearest adjacent site}$$

$$X_v = \text{Probability that any one adjacent site is vacant}$$

Intrinsic diffusivity, which operates independent of any concentration gradient, relates temperature to the random walk theory as shown in Equation (2). Equation (2) relates jump rate to the intrinsic diffusion coefficient. Since this study is bonding similar materials and does not implement an interlayer material, volume diffusion between substrates is largely dependent on random walk to achieve coalescence as there is no strong concentration gradient to direct atom movement.

$$D_A = \frac{1}{6}\alpha^2\Gamma \tag{2}$$

where

$$D_A = \text{Intrinsic diffusivity coefficient of “A” atoms}$$

$$\alpha = \text{Lattice Parameter}$$

Another way to remedy surface imperfections is to add an interlayer material containing melting point depressant constituents [6]. The interlayer, which becomes liquid at bonding temperatures, can serve the purposes of establishing contact between the substrates and by introducing a strong concentration gradient as outlined in Fick’s laws of diffusion. This process is termed Transient Liquid Phase Diffusion Bonding. A strong concentration gradient aids bonding as it directs atom movement at the highly concentrated joint interface [4,5]. While an interlayer material with melting point depressants is advantageous for accomplishing acceptable bonding, it also introduces new elements into the base substrate which can locally change the properties of the material near the weld interface. Insufficient diffusion of melting point depressants can result in a reduction of the base materials melting point at the joint interface. Adding interlayer materials that do not contain melting point depressants, intended to be bonded in the solid state, introduce a strong concentration gradient but do not mitigate challenges associated with achieving intimate contact of mating surfaces and still locally change the composition of the alloy. However, they can offer reduced risk of lowering the melting point of the joint interface.

While elevated temperatures increase jump rate, it also fosters the formation of oxide layers on the substrate’s surface. For this reason, a controlled atmosphere must be maintained to prevent oxides from forming at high temperatures. Hard vacuum is preferred, as oxides often have low vapor pressure and will sublime when subjected to high temperatures at hard vacuum levels. If used, interlayer materials, having a low vapor pressure constituents such as silver, will also sublime at bonding temperature in vacuum. Sublimation of melting point depressant interlayer materials makes bonding in a partial pressure inert atmosphere preferred to prevent vaporized melting

point depressants from contaminating the vacuum furnace over time. In these cases, precautions must be implemented to ensure ultra-high purity of inert gas is used. Moisture content is one consideration that makes bonding in a partial pressure inert atmosphere less preferred than vacuum [7].

The AWS Welding Handbook outlined three discrete stages of the Diffusion Bonding process (shown in Figure 1). The first stage is characterized by plastic deformation of surface peaks and asperities to form the initial boundary. Second stage diffusion involves grain boundary migration. Third stage diffusion describes volume diffusion which entails interfacial boundary elimination, pore closures within individual grains [2]. Initial interface boundary formation of first stage diffusion often results in high angled grain boundaries which have higher boundary energies, relative to low angled grain boundaries. As a result of built-up free energy from plastic deformation and high angled grain boundaries, dynamic recrystallization (DRX) and grain boundary migration occur at the joint interface [8].

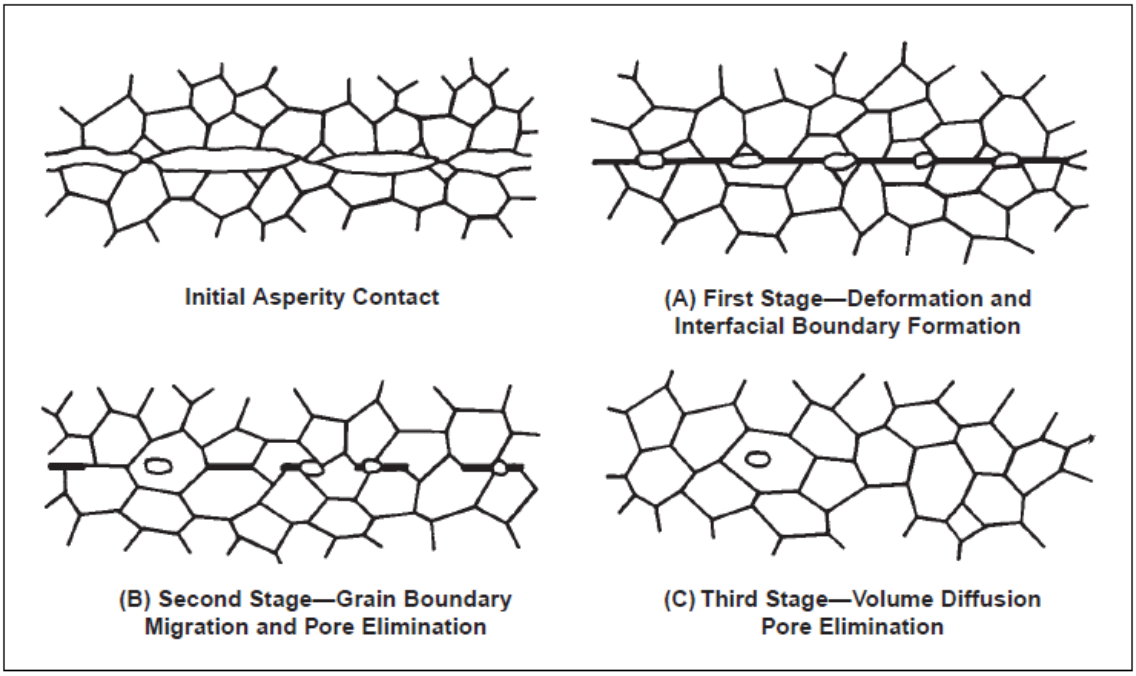

Figure 1. Three Stages of Diffusion [2].

Guoge et al. [9] conducted experiments on diffusion bonding of precipitation hardened Inconel 718 ranging from just below to just above solution heat treatment temperatures. They completed diffusion bonding in a vacuum hot press and utilized higher loading conditions than the scope of this study. Metallographic results of their study showed incomplete recrystallization of the joint interface. Tensile results were shown to increase logarithmically with increased temperature. In a later study, this same author also reported precipitation of δ phase, from the preexisting γ" phase, in weldments bonded below 970 °C (1778 °F) had detrimental effects on tensile properties. δ phase is known to precipitate between 700 °C (1292 °F) and the materials solution temperature of approximately 1000 °C (1832 °F) (see the red curve in Figure 2) [9,10].

Inconel 718 is a solid solution strengthened FCC alloy with additional precipitation strengthening from the intermetallic phases of γ" (Body Centered Tetragonal Ni_3Nb) and trace amounts of γ' (Face Centered Cubic $Ni_3(AL, Ti)$). The alloy was developed in the 1960s by H.L Eiselstein of the International Nickel Company (where the alloy gets its trade name "Inconel" from) and has been extensively used in the aerospace industry due to its availability, versatility, and excellent mechanical properties at elevated operating temperatures [11]. The materials yield strength is inversely related to its grain size, as shown by Hall-Petch relationship. Impact of grain size on tensile strength of Inconel 718 was demonstrated by Ruan et al. [12]. Phases such as δ phase (Orthorhombic Ni_3Nb) and Laves Phase have been shown to increase fatigue life but degrade tensile properties when precipitated, typically at grain boundaries [12–18]. The Time-temperature-transformation (TTT) precipitate diagram (Shown in Figure 2), created by R.G Thompson et al., shows the temperature ranges at which each of the above-mentioned precipitates are formed [17].

Literature reviews show that Alloy 718 has widely been used in industry and extensively researched. It was selected for this study for its availability, for its precipitation hardening characteristics and to determine its mechanical properties bonded at super solvus temperatures without the aid of an interlayer material.

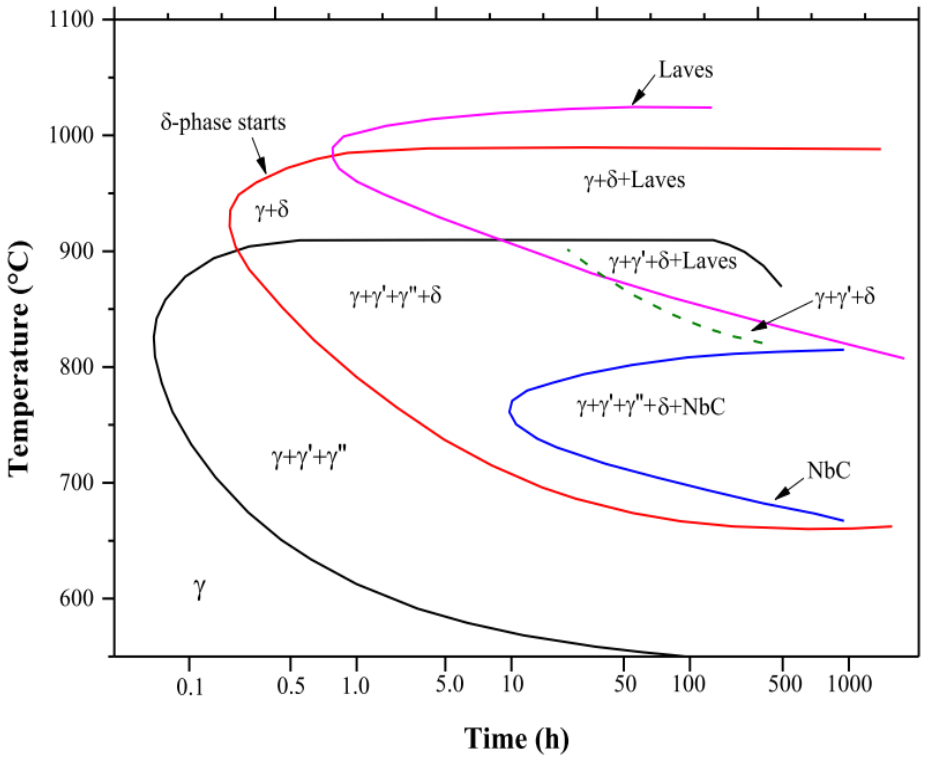

Figure 2. TTT diagram of Inconel 718 (Taken from Thompson et al. [17]).

2. Experimental Procedures

Inconel 718 bar, compliant to AMS5662, was sectioned into 1.25 inch (31.75 mm) long sections with a section saw [16]. After sectioning, samples bond surfaces were polished via general metallographic polishing equipment to 1200 Grit paper. A vibratory polisher was then used to achieve the final surface finish which was systematically varied. Since surface finish is an essential element to the process, a Veeco WYKO NT1100 interferometer was used to measure the microscopic surface finish after polishing. Samples were cleaned in an Acetone bath with ultrasonic agitation for a duration of 15 min. In an attempt to minimize oxide formation, samples were placed into vacuum furnaces within 60 min of final polishing.

Welding took place in a Centorr Vacuum Furnace with an integrated hot press that complied to the requirements of AMS 2750 [19]. The integrated hot press was designed to maintain a constant loading by varying ram displacement. The furnace was equipped with data acquisition technology with thermocouples and sensors integrated to record essential bonding parameters at a sampling rate of two readings/minute for the duration of the bonding cycle. High vacuum levels of 10^{-4} Torr were used until a temperature levels of 500 °C (932 °F) was reached then ultra-high purity argon backfilled the chamber. The furnace operator mistakenly selected the wrong program on SN 5 and completed bonding of this sample under high vacuum. Tungsten tooling blocks were used to minimize tooling distortion and wear. A ceramic spacer was used as an isolator, so that the tooling would not bond to the sample.

Several combinations of bonding parameters were tested and are outlined in Table 1. Since the goal of coalescence without the aid of an interlayer materials, parameters were not varied systematically. Rather they were iteratively varied to establish an acceptable solid state diffusion bond. SN0, being the starting point, was selected based on the materials recrystallization temperature, yield strength (at the temperature and pressure selected), and soak time based on previous production experience. SN1 increased the time at temperature in an attempt to foster grain crossing. SN2 decreased the surface roughness and increased loading to aid in pore closure. SN3 further reduced surface roughness but decreased loading to reduce distortion. One of the key research goals was to have as little distortion as possible, relatively low loading was implemented ranging from 4.65 mpa (675 psi)–11.03 mpa (1600 psi). SN4 increased temperature to further foster grain crossing. SN5, mistakenly bonded in high vacuum, was intended to control grain growth while still achieving grain coalescence. SN6, 7, and 8 were an attempt to control grain growth. Per previous research, bonding temperatures were kept above solution temperature to avoid the precipitation of δ phase [12,14]. Soak times were based on previous experience and literature review [12].

Table 1. Bonding Parameters and Testing Results.

Sample ID	Surface Finish RA µm (µin)		Diffusion Bonding Parameters					
	A	B	Temperature °C (°F)	Soak Time (Hours)	Pressure Mpa (psi)	Atmosphere	ASTM Grain Size Number (Unitless)	Yield Strength Mpa (KSI)
Control	N/A	N/A	N/A	N/A	N/A	N/A	3.77	(148.5)
SN0	N/R	N/R	1175 (2147)	4	4.653 (675)	99.9997% Argon	1.64	-
SN1	7.74 (304.7)	6.04 (237.8)	1175 (2147)	8	4.653 (675)	99.9997% Argon	0.799	-
SN2	4.23 (169.3)	4.64 (182.7)	1175 (2147)	8	11.032 (1600)	99.9997% Argon	0.43	-
SN3	1.76 (69.3)	1.08 (42.5)	1175 (2147)	8	6.895 (1000)	99.9997% Argon	−0.58	-
SN4	0.1 (3.39)	0.09 (3.54)	1225 (2237)	8	5.861 (850)	99.9997% Argon	−1.705	(111.03)
SN5	0.14 (5.51)	0.14 (5.51)	1225 (2237)	5	5.861 (850)	Hard Vacuum	0.082	(143.09)
SN6	0.09 (3.54)	0.12 (4.72)	1225 (2237)	4	5.861 (850)	99.9997% Argon	−2.49	(110.68)
SN7	0.11 (4.33)	0.11 (4.33)	1130 (2066)	4	11.032 (1600)	99.9997% Argon	2.119	(114.54)
SN8	0.097 (3.82)	0.067 (2.637)	1175 (2147)	4	11.032 (1600)	99.9997% Argon	−1.26	(124.478)

- indicates the test was not performed. N/A indicates not applicable. N/R indicates data was not recorded.

After bonding, one metallographic sample, taken transverse to the joint interface, was removed from each sample for evaluation in the as-welded condition. A second metallographic sample was taken after precipitation heat treatment for comparison and for collecting micro hardness measurements. Metallographic samples were prepared by sectioning bonded samples and mounting them in epoxy resin then polishing to 0.05 µm RA, and electrolytically etched at 3 volts for 6–12 s with 10% oxalic. A Keyence VHX-X1 digital microscope was used for metallographic analysis with magnifications ranging from 20× to 1200×. The samples were evaluated to ensure that proper coalescence between the two substrates was achieved with adequate grain boundary migration across the original joint interface and pore closures. Grain size measurements were taken using the Heyne intercept technique and values were converted to ASTM grain size number using the formula shown in Equation (3). Note that this equation allows for a negative ASTM grain size number which is atypical and not generally illustrated in comparative charts. A negative ASTM grain size number indicates a very large grain size. Individual secondary phases were randomly measured to compare sizes between samples.

$$\mathrm{G} = -6.6457 \log \bar{\ell} - 3.298 \tag{3}$$

where

$$\mathrm{G} = \text{ASTM Grain Size Number}$$

$$\bar{\ell} = \frac{\bar{\ell}_{\mathrm{T}}}{\mathrm{PM}}$$

$$\bar{\ell}_{\mathrm{T}} = \text{Total Length of Lines}$$

$$\mathrm{P_I} = \text{Number of Grain Boundaries Intersected}$$

$$\mathrm{M} = \text{Magnification Used}$$

When an acceptable bond was characterized in metallography, the sample was subjected to a two-step precipitation heat treatment in accordance with AMS2774 condition S1750DP in a vacuum furnace [20]. A data acquisition system was used to monitor the heat treatment cycle and ensure compliance with AMS2774 [19]. Since bonding temperatures exceeded the solution heat treat condition, this aging cycle was implemented to precipitate γ" (Ni_3Nb) and γ' (Ni_3Ti) [20]. Even though the temperature ranges were well below the δ phase precipitation curve, shown in Figure 2, argon gas quenching was used to control cooling rates.

A Tescan Vega scanning electron microscope was used to analyze metallographic samples to identify precipitates and look for relevant indications that can be difficult to see with optical metallography. Scanning electron microscopy energy dispersive x-ray spectrometry (SEM-EDS) was used to characterize secondary phase chemical composition. In order to ensure the sample's surface was adequately conductive, mounted samples were gold plated using the sputter technique. Copper tape was also applied to a corner of the sample's surface and then connected to the fixture to ensure conductivity. Samples were observed using both backscatter and secondary emission technique. EDS analysis of precipitates was implemented to characterize the locations of interest and surrounding areas.

The wire EDM process was used to remove miniature flat tensile samples, compliant to ASTM E8, from the weldment with the joint interface located in the approximate center of the gauge (see Figure 3 for reference). The gauge of the single blanked samples was carefully polished by hand with 600 grit sandpaper to remove any recast

layer from the wire EDM process with micro scratches going in the direction of loading. Once recast was removed, the sample was taken back to the wire EDM machine to remove a minimum quantity of 10 samples, 2.616 mm (0.103 in) thick, from the blanked sample. Recast was again carefully removed from the sample by hand polishing with 600 grit sandpaper with micro scratches going in the direction of loading.

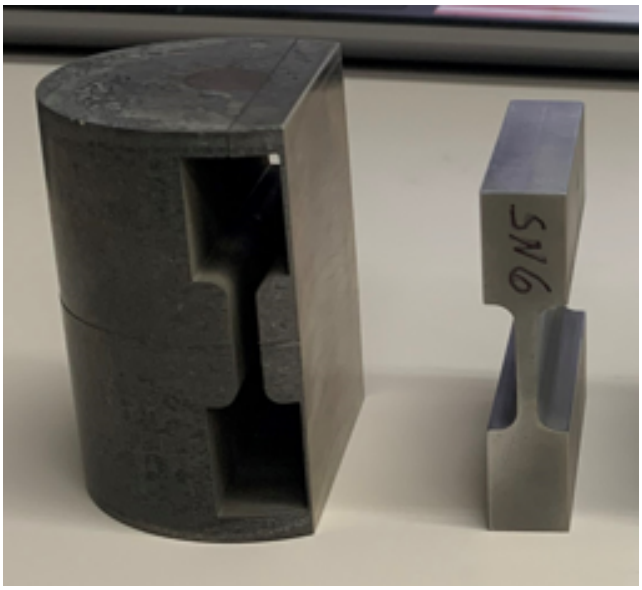

Figure 3. Location of Tensile Samples Relative to Weldment.

Tensile testing was conducted using an Instron load cell in conformance to ASTM E8 at room temperature (see Figure 4 for setup configuration). It was determined that the load cell and tensile samples worked best utilizing crosshead speed controls (ASTM E8 Control Method C) with a strain rate of 0.05 in/in/min which was implemented on all samples tested. A laser extensometer, in conjunction with reflective tape, was used to collect strain data. Ten samples were tested for each experiment to establish a statistical minimum dataset [21].

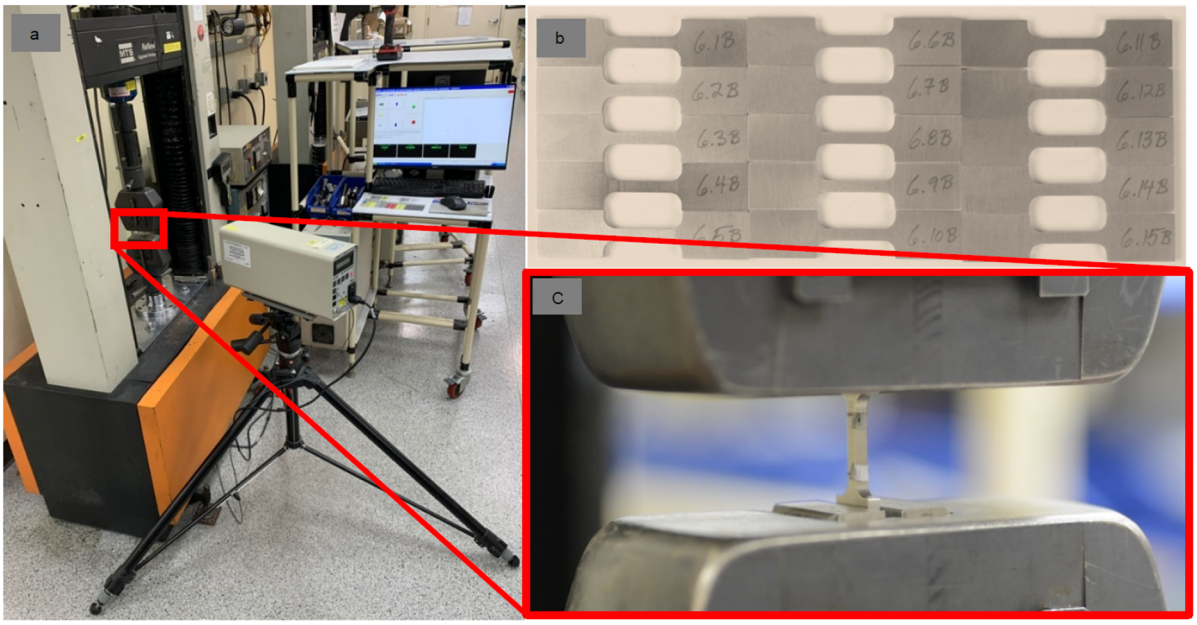

Figure 4. Tensile Testing Configuration. (**a**) Instron Tensile Tester with Epsilon Laser Extensometer. (**b**) Miniature Flat Tensile Sample Profile View (8× Magnification). (**c**) Miniature Flat Tensile Sample in Testing Jaws (5× magnification).

A Struers Duramin-40 AC1 was used to collect Vickers 0.05 kg (HV0.05) microhardness data. Four traverses (across the joint interface) per sample were taken perpendicular to the joint interface, each containing five indentions for a total of twenty microhardness readings per weldment. The third row of indentations of each traverse was centered on the joint interface. Each indentation was manually checked to verify proper measurements of the indentation. The values were averaged to obtain the weldments microhardness.

To have a control material for comparison, one unbonded base material substrate was subject to a super solvus solution heat treatment and two step precipitation heat treated in accordance with AMS2774 condition S1750DP and subjected to metallography, hardness, and tensile testing (ten samples). The same sample preparation procedures and sample sizes described above for metallography, microhardness and tensile samples was used on this control sample as were used on the bonded samples.

3. Results and Discussion

First stage mechanism suggests that free surfaces quickly begin sharing atoms where contact is made and becomes more restricted to atom movement, similar to diffusion within the bulk, as bonds are formed. Grain boundary diffusion rates dominate at lower temperatures due to highly disordered packing resulting in a lower activation energy barrier [4]. Grain boundary migration, driven by the minimization of boundary energy, tend to align and result in elimination of the joint interface. This alignment of grain boundaries is described as second stage diffusion shown in Figure 1. Third generic diffusion bonding process stage involves plastic deformation allowing intimate contact between surfaces and forces unbonded surfaces and micro pores to be eliminated. Complete coalescence consists of two materials that are nearly indistinguishable from one another where the joint interface cannot be easily seen.

Looking at the metallographic images of the bonds and relating to the parameters that were used for each test, it appears that surface roughness plays a very critical role to the extent that it overshadows other parameters such as temperature and pressure. As seen in Figure 5, the joint interface only starts to disappear when the surface roughness is reduced to 0.2 µm. Metallographic inspection revealed that varying stages of diffusion had taken place as outlined in Figure 1 [2]. Sn0 achieved stage 1 diffusion, since initial contact was made but grain boundaries were not aligned. Sn1, 3 had some grain crossing which by definition achieves stage 2 diffusion. SN 2 had good grain crossing and pore closure, however the sample had excessive distortion. It was not until the average surface roughness (RAµm) was decreased to under 0.2 µm (7.874 µin) that acceptable stage 3 diffusion was achieved on samples 4, 5, 6, 7, and 8.

As temperature increases, mobility of the atoms increases resulting in higher diffusion rates as dictated by Ficks Laws. However, increasing temperature can also result in recrystallization and grain coarsening at temperatures above recrystallization temperature for Inconel 718. Recrystallization temperature for Inconel 718 varies and it could be as low as 1150 °C. Samples bonded at 1225 °C (2237 °F) were consistent with this and had excellent diffusion and pore closure. However, as expected grain recrystallization and coarsening also occurred as these samples had a negative ASTM grain size number which indicates very large grains. Experiments (SN7 and SN9) were conducted at lower temperatures, 1130 °C (2066 °F) and 1175 °C (2147 °F) respectively, with higher loading intended to achieve intimate contact between substrates faster. These tests resulted in a positive ASTM grain size number while still achieving adequate coalescence and marginal micro pore closure.

SEM-EDS line scans were used to characterize any residual oxide layer on samples bonded in high vacuum and in argon atmosphere. Line scan results did not show an increase in oxygen content indicating that no significant oxide layer was present. This test is considered less reliable since SEM-EDS does not reliably resolve elements with an atomic number below 10. A closer look at the microstructure through SEM-EDS analysis revealed existence of large Niobium rich carbide and Titanium rich nitride precipitates, throughout all the samples including the base material as well as bonded samples. It was observed that in some instances, these carbides were linearly aligned with the roll direction, as shown in Figures 5 and 6. Ostwald Ripening, of Niobium rich carbide and Titanium rich nitride precipitates was observed in all processed samples, including the unbonded base material in the precipitation heat treated condition, to varying degrees [12]. Precipitates displayed elevated levels of Nb and C in the form of white particles in the matrix while black precipitates contained Ti and N as shown in Figure 6. Ostwald Ripening is a diffusion-controlled precipitation growth mechanism where large precipitates grow larger at the expense of smaller precipitates, driven by the higher interfacial energies associated with smaller precipitates. It is shown that elevated temperatures are required to achieve volume diffusion also expedites diffusion required to cause undesired precipitation growth. This effect can theoretically deplete the crystalline lattice of valuable elements required to form γ” and γ’. This is further complicated since Niobium and Titanium are extremely reactive elements and are incredibly stable in NbC and TiN form, making dissolving these precipitates nearly impossible. Ruan et al. showed that dissolving NbC precipitates required temperatures near Inconel 718’s melting temperature, 1280 °C (2340 °F). The study showed that TiN would still exist at liquid temperatures and would gradually be dissolved by liquidus phases [12].

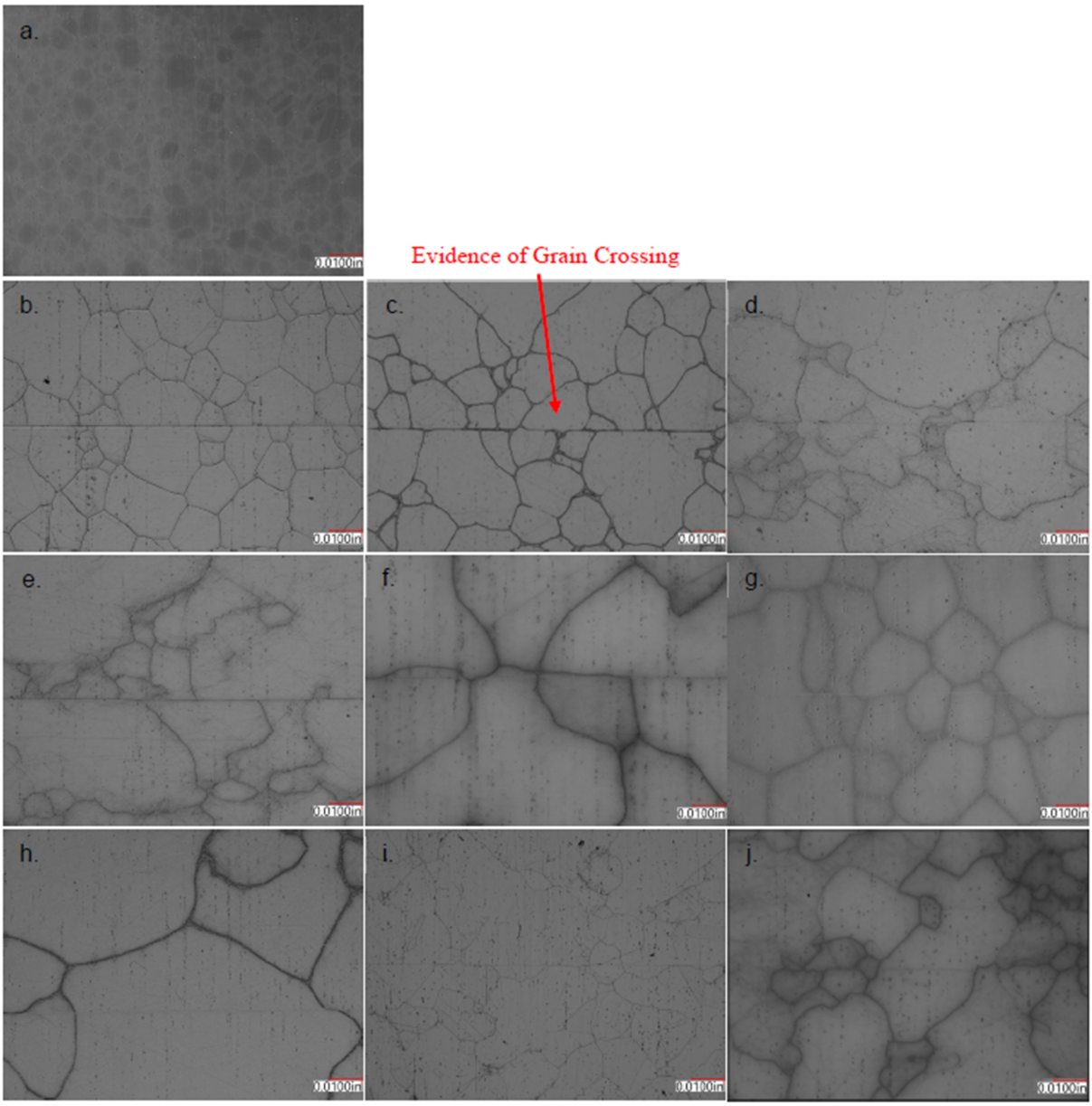

Figure 5. Metallography Transverse to Joint Interface. (**a**) Control sample (Unbonded base material in the aged condition), ASTM Grain Size Number: 3.77. (**b**) SN0 (Bonded at 1175 °C for 4 h, RA was not recorded), ASTM Grain Size Number: 1.64. (**c**) SN1 (Bonded at 1175 °C for 8 h, RA was <7.74 µm), ASTM Grain Size Number: 0.799. (**d**) SN2 (Bonded at 1175 °C for 8 h, RA was<4.64 µm), ASTM Grain Size Number: 0.43. (**e**) SN3 (Bonded at 1175 °C for 8 h, RA was <1.76 µm), ASTM Grain Size Number: −0.58. (**f**) SN4 (Bonded at 1225 °C for 8 h, RA was <0.1 µm), ASTM Grain Size Number: −1.705. (**g**) SN5 (Bonded at 1225 °C for 5 h, RA was <0.14 µm), ASTM Grain Size Number: 0.082. (**h**) SN6 (Bonded at 1225 °C for 4 h, RA was <0.12 µm), ASTM Grain Size Number: −2.49. (**i**) SN7 (Bonded at 1175 °C for 4 h, RA was <0.11 µm), ASTM Grain Size Number: 2.119. SN8 (Bonded at 1175 °C for 4 h, RA was <0.11 µm), ASTM Grain Size Number: −1.26.

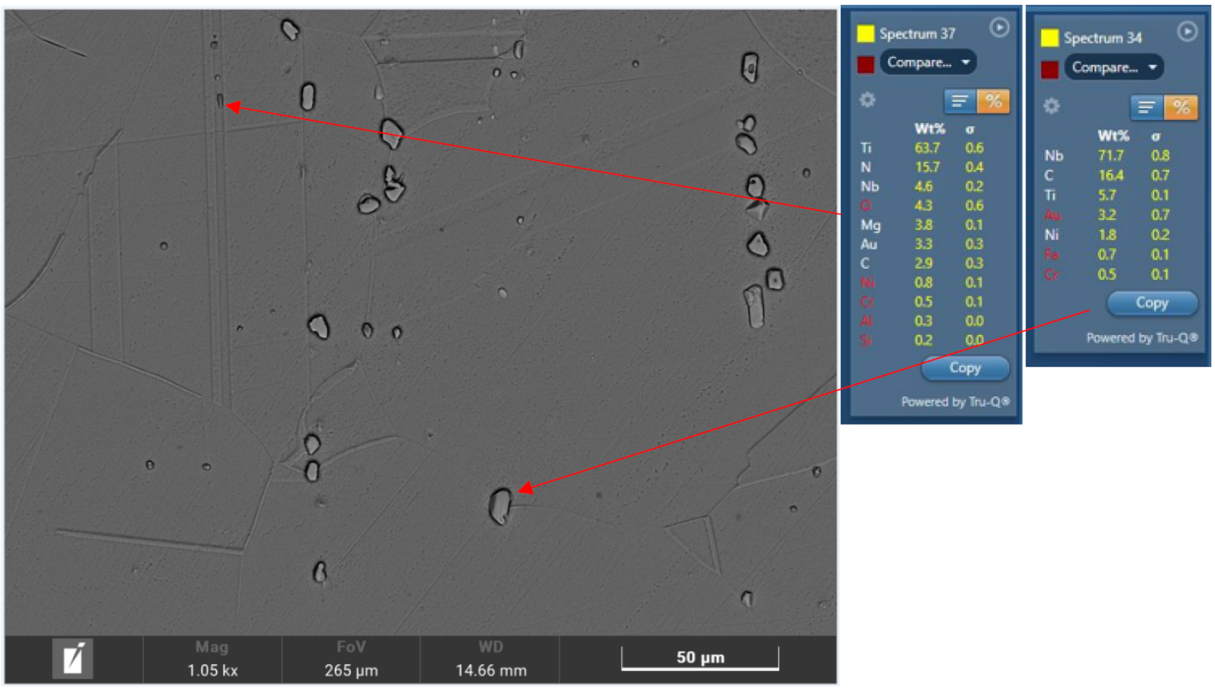

Figure 6. SEM Analysis of Precipitates in Unbonded Base Material.

A proper balance between achieving coalescence at the joint interface and maintaining a fine grain size in the substrate as well as avoiding Ostwald Ripening is a challenge as diffusion, which is a temperature driven mechanism, is the cause for all these phenomena. It can be concluded that some amount of grain growth would be required to achieve volume diffusion and grain migration across the joint interface, since it is only possible to refine grain size on nickel-based alloys through cold working. This effect can be accounted for in the design's calculations.

As a result, a reduction in mechanical properties must be considered due to grain growth per the Hall-Petch theory (shown in Equation (4)) and diffusion-controlled Ostwald Ripening [22]. Figure 7 shows the Hall-Petch relationship plotted against the experimental data collected. Friction stress (σ_y) of 700 and 900 were used to showcase varying levels of the precipitation heat treatment effectiveness and were taken from literature. The Materials strengthening coefficient (k_y) of 1200 was also obtained from literature [23]. The relationship showing a decrease in yield strength due to increased grain size is observed. It is also observed that the materials' strengthening coefficient experiences varying level of strengthening even though all samples were aged with the same heat treatment. This point is further complicated in Inconel 718 since the detrimental δ phase has been shown to precipitate between 700 °C (1292 °F)–1000 °C (1832 °F), which bounds the lower temperature at which diffusion bonding would be practical without complex bonding temperature cycles [22]. It should be noted that some data indicates that δ phase could be leveraged to control grain growth [24].

$$\sigma_y = \sigma_0 + \frac{k_y}{\sqrt{d}} \tag{4}$$

where

$$\sigma_0 = \text{friction stress } \{\text{resistance of dislocation movement in lattice}\}$$

$$k_y = \text{material strengthening coefficient}$$

$$d = \text{average grain diameter}$$

Table 2 presents the mechanical tests were conducted at room temperature to the point of failure to evaluate the elastic and plastic mechanical behavior. The base material displayed an average Youngs Modulus of 23 Mksi, yield strength of 1013.94 Mpa (148.57 ksi) at 2% offset, ultimate tensile strength of 1243.12 Mpa (181.4 ksi), and 31.84% elongation which closely align with the published data of AMS5662 [16]. The base material's tensile properties were very consistent showing a yield strength standard deviation of 1.57.

Table 2. Tensile Testing Results for all samples.

Tensile Testing Overview				
Sample	**Yield**	**UTS (KSI)**	**Elongation %**	**Fracture Type/Location**
T4.1	108.6	125.1	27.6	Ductile/Gauge
T4.2	105.5	136.3	26.6	Ductile/Gauge
T4.3	115	134.9	22.00	Ductile/Gauge
T4.4	107.80	135.2	25.00	Ductile/Gauge
T4.5	91.2	136	24	Brittle/Joint Interface
T4.6	120.8	132.2	20	Ductile/Gauge
T4.7	117.2	134.2	20.8	Ductile/Gauge
T4.8	119.5	130.8	***	Ductile/Gauge
T4.9	107.9	128.2	26	Ductile/Gauge
T4.10	116.8	128.6	***	Ductile/Gauge
T5.1	140.2	161.7	***	Brittle/Joint Interface
T5.2	132.5	159.8	15.2	Brittle/Joint Interface
T5.3	144.6	162.7	19.8	Brittle/Joint Interface
T5.4	142.2	158.3	14	Brittle/Joint Interface
T5.5	144.4	162.1	15	Brittle/Joint Interface
T5.6	143.2	159.5	14	Brittle/Joint Interface
T5.7	142.4	162.2	17	Brittle/Joint Interface
T5.8	144.5	158.3	8	Brittle/Joint Interface
T5.9	143.9	155	10	Brittle/Joint Interface
T5.10	153	171	15	Brittle/Joint Interface
T6.1	***	122.03	***	Ductile/Gauge
T6.2	112.9	129.90	20	Ductile/Gauge
T6.3	105.9	118.00	21.7	Ductile/Gauge
T6.4	117.6	132.90	18	Brittle/Joint Interface
T6.5	118.4	126.30	6.8	Brittle/Joint Interface
T6.6	***	127.90	19.8	Brittle/Joint Interface
T6.7	106.8	120.80	18.8	Brittle/Joint Interface
T6.8	106.5	124.30	23.6	Ductile/Gauge
T6.9	109.3	115.30	15.8	Brittle/Joint Interface
T6.10	108	116.70	20.6	Ductile/Gauge
T7.1	116.2	140.6	16.6	Brittle/Joint Interface
T7.2	112.4	143.1	29	Brittle/Joint Interface
T7.3	115.3	139.4	19	Brittle/Joint Interface
T7.4	115.4	138.7	19.2	Brittle/Joint Interface
T7.5	112.6	138.5	19.2	Brittle/Joint Interface
T7.6	114.5	146.5	43.2	Ductile/Gauge
T7.7	114.3	131.7	15.6	Brittle/Joint Interface
T7.8	115.5	137.6	19	Brittle/Joint Interface
T7.9	115.2	145	25	Brittle/Joint Interface
T7.10	114	144.3	26	Brittle/Joint Interface
T8.1	125.5	147.5	29.4	Brittle/Joint Interface
T8.2	122.1	147.7	26.5	Brittle/Joint Interface
T8.3	125.9	147.3	22	Brittle/Joint Interface
T8.5	118.3	146.5	25	Brittle/Joint Interface
T8.6	125.3	147.1	19.4	Brittle/Joint Interface
T8.7	125.8	146.5	20.7	Brittle/Joint Interface
T8.8	124.3	144.8	16	Brittle/Joint Interface
T8.9	124.1	147.2	20	Ductile/Gauge
T8.10	129	150.1	18	Ductile/Gauge

*** Indicates an error occurred with the laser extensometer and data was not recorded.

Diffusion bonding parameters had a drastic impact on the weldment's mechanical properties indicating that rigorous development and qualification of parameter must be considered in the development process. All samples bonded in argon atmosphere displayed reduced yield, UTS and elongation while samples bonded in hard vacuum (where the argon atmosphere was not turned on by mistake) (SN5) displayed yield strengths similar to the base material. In most samples brittle fracture occurred in the joint interface exhibiting a lower ductility. Figure 8 displays representative average stress strain curves for each weldment. These representative curves are based on the average of all ten tensile samples tested from each weldment. Figure 8 also shows the yield and ultimate tensile strength mean and variants in the box and whisker diagrams. All samples displayed strain hardening to varying extents. The reduced strength can be theoretically related to the Hall-Petch effect due to grain coarsening that occurs during bonding. Metallography of the control sample displayed significantly smaller grain sizes than any of the samples bonded.

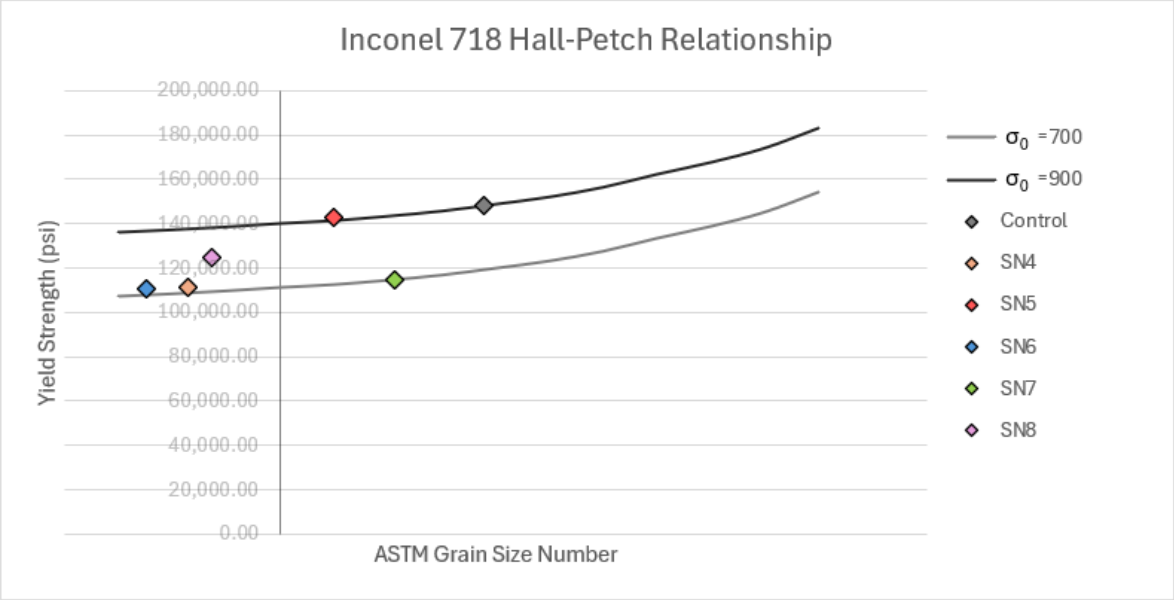

Figure 7. Experimental Average Yield values V.S. Theoretical Hall-Petch Relationship.

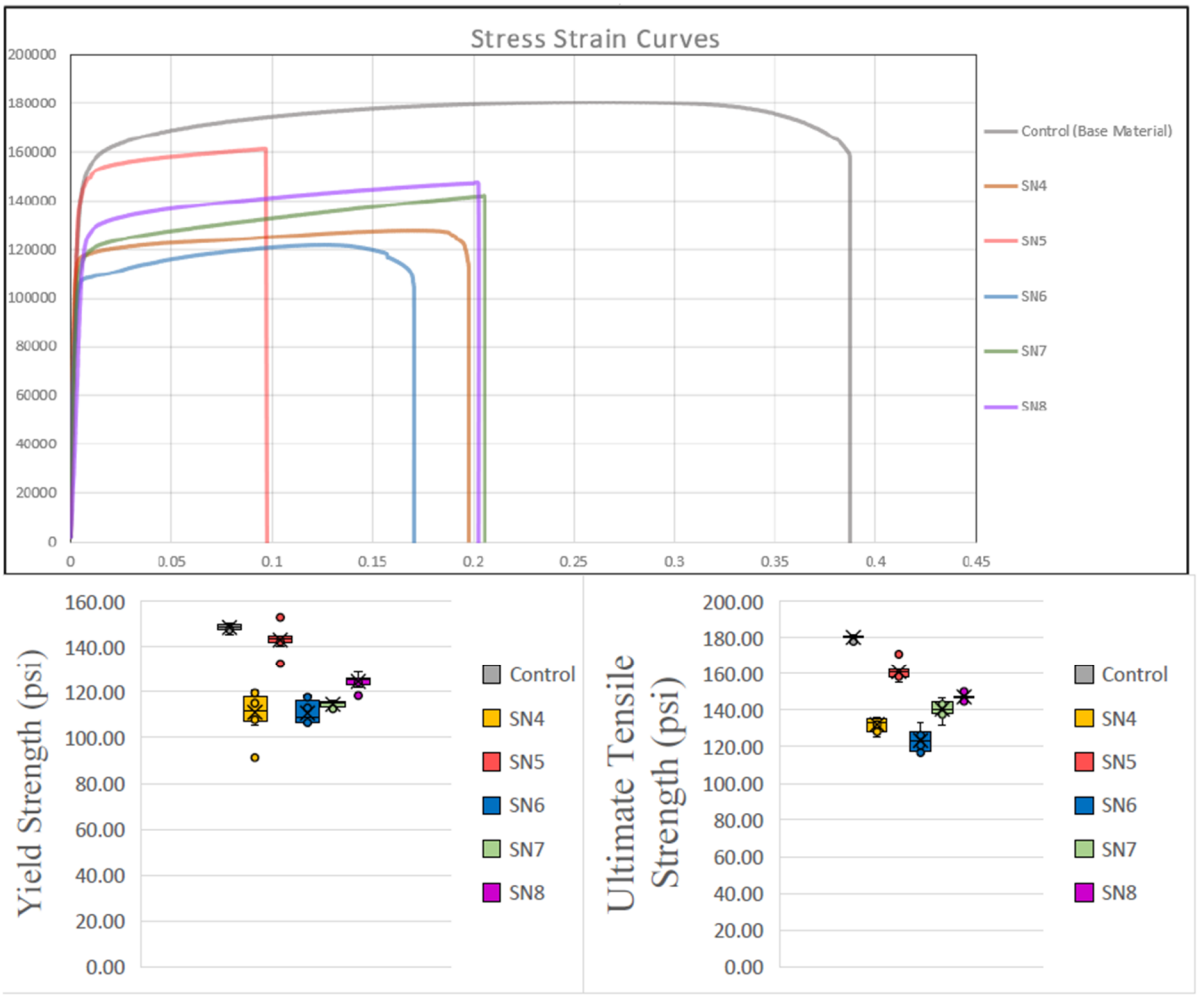

Figure 8. Representative Average Stress Strain Curves of Weldment Population and Their Respective Standard Deviations. (X axis: Strain (in/in), Y axis: Stress (psi)).

Optical microscopic analysis of tensile samples metallography, shown in Figure 9, indicated that plastic deformation of all samples appears to be uniform through the tensile samples gauge. This is consistent with the theoretical advantage of diffusion welding having uniform mechanical properties, similar to the base material. Samples that displayed brittle fracture had significantly less plastic deformation due to the premature failure in the

joint interface. Premature fracture could theoretically reduce ultimate tensile strength values due to the test being interrupted before samples become fully strain hardened. These metallography samples give a clear picture of the amount of grain growth that each parameter set consisted of. It shows that the tensile strength of the material is inversely related to the grain size [12,22].

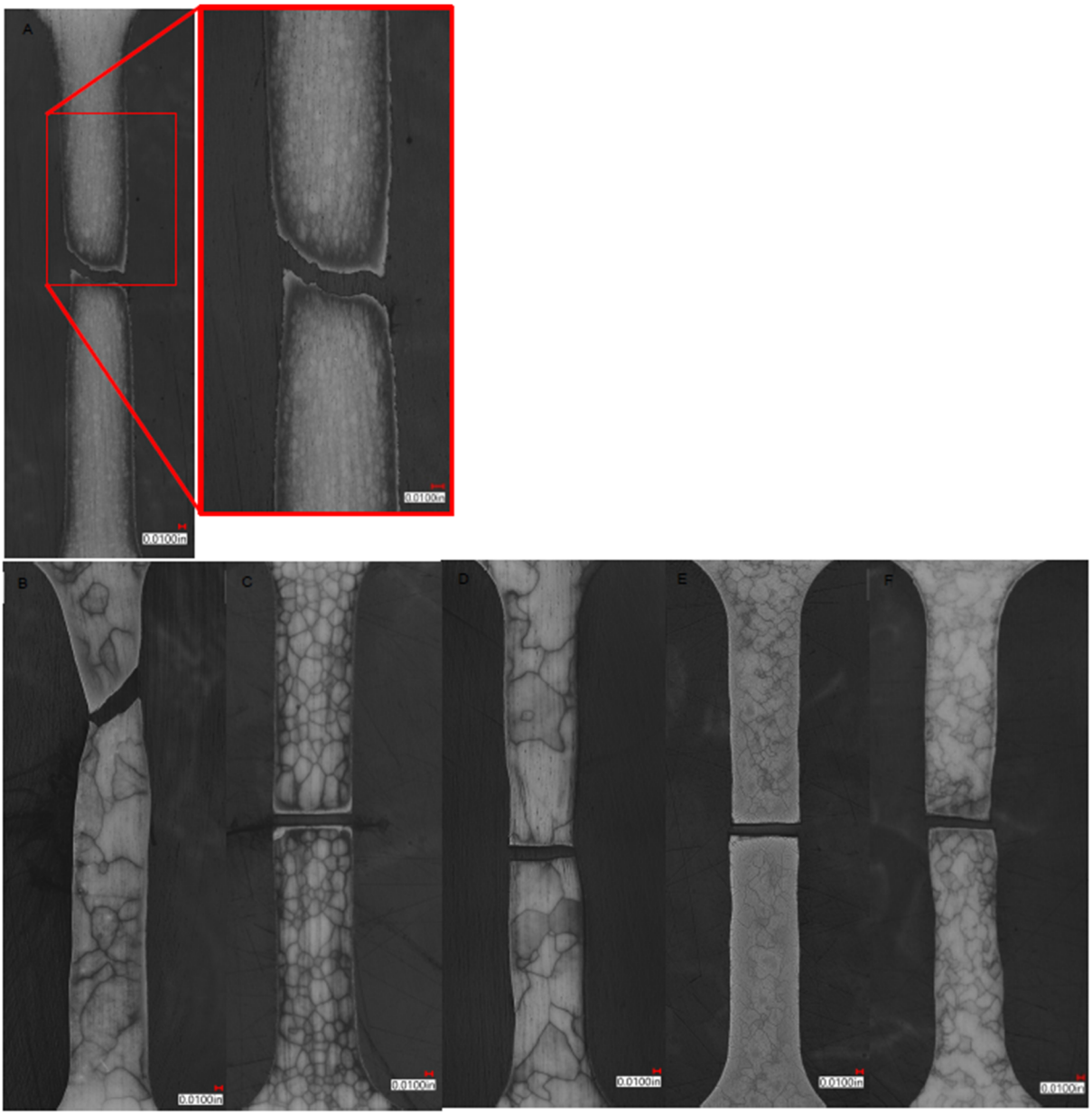

Figure 9. Tensile Sample Metallographic Evaluation of Bonded Joints at 20× Magnification. (**a**) Control sample. (**b**) SN4 (Bonded at 1225 °C for 8 h, RA was <0.1 µm). (**c**) SN5 (Bonded at 1225 °C for 5 h, RA was <0.14 µm). (**d**) SN6 (Bonded at 1225 °C for 4 h, RA was <0.12 µm). (**e**) SN7 (Bonded at 1130 °C for 4 h, RA was <0.11 µm). (**f**) SN8 (Bonded at 1175 °C for 4 h, RA was <0.11 µm).

Fractography was conducted on all samples to evaluate the underlying microstructural causes of fracture. Fracture behavior of the control tensile samples displayed ductile failure in the gauge of the specimen with a shear lip of approximately 45°. Fracture behavior of bonded samples varies from ductile fracture (in the base material) and brittle fracture at the joint interface. Almost all tensile samples of SN4 and 6 displayed ductile fracture in the base material. SN7 and SN8 had several samples display ductile facture, although most failed in the bond with a brittle type of fracture. Even though SN5 displayed the highest yield strengths of the bonded samples, all tensile tests displayed brittle fracture in the joint interface. This behavior appeared to be a direct result of the grain size, and bond quality. Finer grain size assisted the material in achieving higher yield strength. Fractured Nb rich precipitates were also found in the fracture surface analysis, as shown in Figure 10. All samples, including the base material, displayed the Nb rich precipitates with fracture going through the precipitate. This indicates that the

precipitates are pinning grain boundaries and dislocations to some degree and assisting in strain hardening [14]. The size of these precipitates, however, varied dramatically.

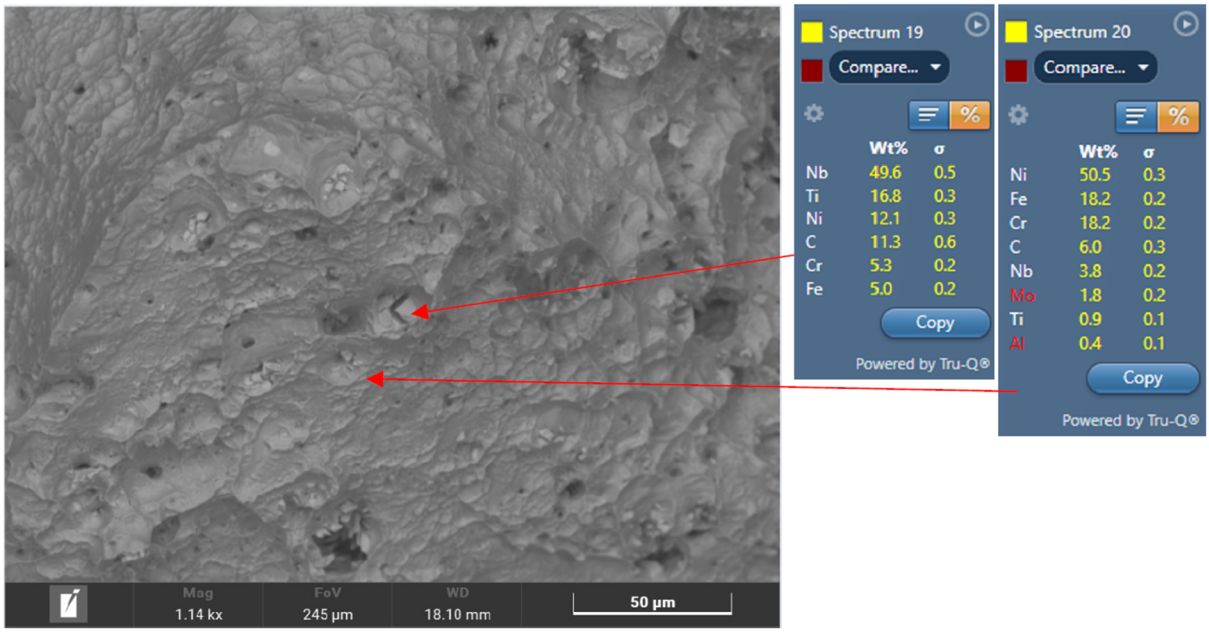

Figure 10. SEM Analysis of Fractured Surface (SN6).

Hardness tests conducted to evaluate the local mechanical properties of the samples showed variations of the hardness due to variation of the parameters. Base material had an average hardness value of 434.81 HV.5. Weldment bonded in hard vacuum (in the precipitation heat treated condition) displayed an average hardness value of 429.72. However, significantly lower values were recorded on samples bonded in argon atmosphere ranging from 376.83 to 408.73. Figure 11, compares each of the sample's average, range of standard deviations of hardness data. All samples displayed significantly higher hardness values in the aged condition than in the as welded condition. Theoretically, this suggests that aging could have caused varying levels of γ" and γ' [25,26]. While the leading theory for the reduced hardness is less precipitation of γ" and γ', due to precipitation forming elements being consumed in large Nb and Ti precipitates via Ostwald Ripening, large grain sizes can also provide some explanation. The placement of the indentation was random and automated, meaning that samples with smaller grains had a higher likelihood of sampling near a grain boundary, which is known to generally have higher hardness values due to precipitates forming at grain boundaries and increased dislocation densities.

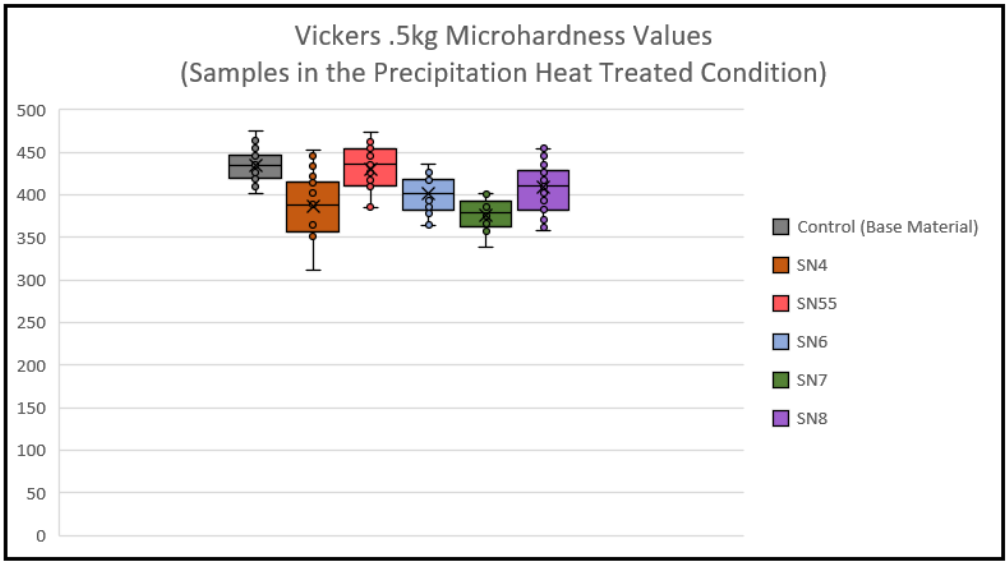

Figure 11. Vickers 0.5kg Hardness Results of Weldments in the Precipitation Heat Treated Condition.

4. Conclusions

Solid state diffusion bonding Inconel 718 to itself at super solvus temperature was studied to establish the effects of the bonding process on the bond formation, grain coalescence and bond's mechanical properties. This information is desired to establish challenges associated with solid state bonding without the aid of an interlayer material.

Literature review showed that bonding at super solvus temperatures would be needed to ensure that detrimental precipitation phases, such as Laves and δ phase, were not formed. Literature and experimental data showed that maintaining mechanical properties of solid-state diffusion bond depends on stringent controls of the surface finish prior to assembly, and maintaining a proper balance of achieving volume diffusion while minimizing grain growth. This research showed that achieving complete coalescence of grains is possible at the expense of refined grain sizes, hence sacrificing the mechanical strength. This increase in grain size decreases the yield and ultimately tensile strength of the material as outlined by Hall-Petch.

Metallurgical testing of all samples showed large Niobium and Titanium rich precipitates linear aligned with the direction of material roll. While these precipitates were observed in all samples, they were significantly smaller in the base material sample. Ostwald Ripening describes the diffusion-controlled growth process of large precipitates at the expense of smaller precipitates. It is hypothesized through theory and literature review that this phenomenon depleted the crystalline lattice of precipitation forming elements needed to form the strengthening intermetallic phases γ" and γ'.

Author Contributions

R.A.: conceptualization, visualization, methodology, performing experiments, writing—original draft preparation; L.L.: supervision, technical input, writing—reviewing and editing. All authors have read and agreed to the published version of the manuscript.

Funding

This research was funded by National Science Foundation grant number 2152254 and the Office of Naval Research grant number N000142512218.

Institutional Review Board Statement

Not applicable.

Informed Consent Statement

Not applicable.

Data Availability Statement

Not applicable.

Acknowledgments

Honeywell Aerospace Technologies allowed the use of their research hot press vacuum furnace and laboratory equipment to support this research. The author is especially thankful to Lindsay Angell for supporting the research efforts and proofreading the rough draft. Chloe Faust provided significant support performing the grain size measurement calculations and for compiling the large amounts of bonding, heat treatment and testing data. John Perek, Camden Brooks, Mark Carroll, and Brent Widder were great consultation resources that helped troubleshooting issues and give guidance on testing.

Conflicts of Interest

The authors declare no conflict of interest.

Use of AI and AI-Assisted Technologies

Grok AI was used to review the paper for spelling, grammar, and typographical errors.

References

1. Kazakov, N.F. Diffusion Bonding of Materials. In *Diffusion Bonding of Materials*; Pergamon Press Inc.: Elmsford, NY, USA, 1985; pp. 10–16. https://doi.org/10.1016/B978-0-08-032550-7.50005-9.
2. Maitland, S.C.; Hall, P.; Zhou, Y.N. Diffusion Welding and Diffusion Brazing. In *Welding Handbook*; The American Welding Society: Miami, FL, USA, 2007. Vol. 3, Part 2.
3. Garrett, B.R.; Blank, G.F.; Ranadive, A.J. *Broad Applications of Diffusion Bonding*; NASA Technical Reports Server; NASA: Washington, DC, USA, 1966.
4. Porter, D.A.; Easterling, K.E.; Sherif, M.Y. *Phase Transformations in Metal and Alloys*; CRC: Boca Raton, FL, USA, 2009.
5. Helmut, M. *Diffusion in Solids*; Springer: Berlin/Heidelberg, Germany, 2007.
6. Shirzadi, A.A. *Diffusion Bonding Aluminium Alloys and Composites*; King's College Cambridge: Cambridge, UK, 1997.
7. American Welding Society. C3 Committee on Brazing and Soldering; American Welding Society: Miami, FL, USA, 2007.
8. Doherty, R.D.; Hughes, D.A.; Humphreys, F.J.; et al. Current Issues in Recrystallization: A Review. *Mater. Sci. Eng. A* **1997**, *238*, 219–274.
9. Guoge, Z.; Chandel, R.S.; Pheow, S.H.; Hoon, H.H. Effect of Bonding Temperature on the Precipitation of δ Phase in Diffusion Bonded Inconel 718 Joints. *Mater. Manuf. Process.* **2006**, *21*, 453–457.
10. Zhang, G.; Chandel, R.S.; Seow, H.P. Solid State Diffusion Bonding of Inconel 718. *Science and Technology of Welding and Joining* **2001**, *6*, 235–239.
11. Eiselstein, H.L. Age-Hardenable Nickel Alloy (718). US 3,046,108, 24 July 1962.
12. Ruan, J.J.; Ueshima, N.; Oikawa, K. Phase Transformations and Grain Growth Behaviors in Superalloy 718. *J. Alloys Compd.* **2018**, *737*, 83–91.
13. Lippold, J.C. *Welding Metallurgy and Weldability of Nickel-Base Alloys*; Wiley: Hoboken, NJ, USA, 2009.
14. Anderson, M.; Thielin, A.-L.; Bridier, F.; et al. δ Phase Precipitation in Inconel 718 and Associated Mechanical Properties. *Mater. Sci. Eng. A* **2017**, *679*, 48–55.
15. Huda, Z.; Zaharinie, T.; Metselaar, H.S.C.; et al. Kinetics of Grain Growth in 718 Ni-Base Superalloy. *Arch. Metall. Mater.* **2014**, *59*, 847–852.
16. SAE International. *AMS5662: Nickel Alloy, Corrosion- and Heat-Resistant, Bars, Forgings, Rings, and Stock for Forgings and Rings, 52.5Ni - 19Cr - 3.0Mo - 5.1Cb (Nb) - 0.90Ti - 0.50AI - 18Fe, Consumable Electrode or Vacuum Induction Melted, 1775 °F (968 °C) Solution Heat Treated, Precipitation-Hardenable*; SAE International: Warrendale, PA, USA, 2024. https://doi.org/10.4271/AMS5662P.
17. Thompson, R.G.; Dobbs, J.R.; Mayo, D.E. The Effect of Heat Treatment on Microfissuring in Alloy 718. *Weld. J. Res. Suppl.* **1986**, 65, 299–304.
18. Cazic, I. *Coaxial Laser Wire Additive Manufacturing of Inconel 718*; Université de Lorraine: Nancy, France, 2022.
19. SAE International. *Pyrometry*; SAE International: Warrendale, PA, USA, 2024. https://doi.org/10.4271/AMS2750.
20. SAE International. *AMS F Corrosion and Heat Resistant Alloys Committee. Nickel Alloy, Heat Treatment Nickel Alloy and Cobalt Alloy Parts*; SAE International: Warrendale, PA, USA, 2021. https://doi.org/10.4271/AMS2774.
21. ASTM International. *E28 Committee. Test Methods for Tension Testing of Metallic Materials*; ASTM International: West Conshohocken, PA, USA, 2025. https://doi.org/10.1520/E0008_E0008M-24.
22. Hall, E.O. The Deformation and Ageing of Mild Steel: III Discussion of Results. *Proc. Phys. Soc. Sect. B* **1951**, *64*, 747–753.
23. Li, C.; Tian, Y.; Chen, Y.; et al. Hierarchical Layered and Refined Grain Structure of Inconel 718 Superalloy Produced by Rolling-Assisted Directed Energy Deposition. *Addit. Manuf. Lett.* **2021**, *1*, 100009. https://doi.org/10.1016/j.addlet.2021.100009.
24. Azadian, S.; Wei, L.-Y.; Warren, R. Delta Phase Precipitation in Inconel 718. *Mater. Charact.* **2004**, *53*, 7–16.
25. Zhang, Y.; Lan, L.; Zhao, Y. Effect of Precipitated Phases on the Mechanical Properties and Fracture Mechanisms of Inconel 718 Alloy. *Mater. Sci. Eng. A* **2023**, *864*, 144598.
26. Mignanelli, P.M.; Jones, N.G.; Pickering, E.J.; et al. Gamma-Gamma Prime-Gamma Double Prime Dual-Superlattice Superalloys. *Scr. Mater.* **2017**, *136*, 136–140.